Oxidation and tensile behavior of ferritic/martensitic steels after exposure to lead-bismuth eutectic

Oxidation and tensile behavior of ferritic/martensitic steels after exposure to lead-bismuth eutectic

Jian Liu[a,b], Quanqiang Shi[a,b], He Luan[a,b], Wei Yan[a], Wei Sha[c], Wei Wang[a], Yiyin Shan[a], Ke Yang[a,*]

[a]Key Laboratory of Nuclear Materials and Safety Assessment, Institute of Metal Research, Chinese Academy of Sciences, Shenyang 110016, China

[b]University of Chinese Academy of Sciences, Beijing 100049, China

[c]School of Planning, Architecture and Civil Engineering, Queen's University Belfast, Belfast BT9 5AG, UK

*Corresponding author. Tel.: +86 24 23971628; E-mail address: kyang@imr.ac.cn (Ke Yang)

Abstract: Two ferritic/martensitic steels, T91 steel and newly developed SIMP steel, were subject to tensile test after being oxidized in the liquid lead-bismuth eutectic (LBE) at 873 K for 500 h, 1000 h and 2000 h. Tensile tests were also carried out on the steels only thermally aged at 873 K. The result shows that thermal aging has no effect. Exposure to LBE at 873 K leads to a slight decrease in strength, but a large decrease in elongation when tested at 873 K. When tested at 873 K after 2000 h exposure, the tensile strength of T91 decreases slightly, and elongation from 39% to 21%. For SIMP, the decreases are slightly and from 44% to 28%, for tensile strength and elongation, respectively. The room temperature strength has slightly larger percentage reductions after the LBE exposure, but the elongation changes little.

Keywords: electron microscopy; light microscopy; steel; oxidation; mechanical characterization; fracture

1. Introduction

The concept of accelerator driven subcritical (ADS) system was proposed to transmute highly radioactive nuclear waste [1]. In the ADS system, the protons flow is accelerated by the accelerator to fire on a spallation target. The spallation target is used to produce neutrons to transmute the long-lived nuclear wastes into short lifetime elements [2, 3]. Generation 4 lead cooled fast reactors (LFR) and lead-bismuth eutectic (LBE) or Pb cooled ADS system would however strongly prefer cladding and duct materials to be able to withstand high dose irradiation, 200 dpa and above, to allow for higher burn-up [4]. The cladding materials of ADS will serve in harsh conditions, such as neutron irradiation, high temperature and corrosion environment. The compatibility of structural materials with liquid metal has become a critical issue in the ADS system design.

T91 steel has good swelling resistance and superior creep properties [5]. SIMP steel is a new ferritic/martensitic (F/M) steel developed by Institute of Metal Research and Institute of Modern Physics, Chinese Academy of Sciences. The dissolution limit of Ni in LBE is high, which increases with temperature, resulting in serious attack of dissolution corrosion [6]. Therefore, the content of Ni in the structural materials must be controlled carefully to ease the dissolution corrosion attack of LBE. Removing LBE soluble elements like Ni from the

structural material could improve the oxidation resistance while keeping the same Cr content [7]. Following this idea, a new kind of steel named SIMP was developed as the candidate material for ADS. The Ni component is replaced by Ta in SIMP. The higher Si and Cr contents provide SIMP with good oxidation resistance.

However, the F/M steels are prone to liquid metal embrittlement (LME) [8-12]. The premature failure of structural material is unacceptable for the long-term safe operation. Slow strain rate testing (SSRT) [13, 14] shows only slightly reduced strength but significantly lower ductility, similar to the present study, in fact, as will be shown in this paper. This does not necessarily imply premature failure. The risk is that, if some mechanical overload occurs, the grace period until failure may be quite short. Creep and stress rupture may be another story. The chance of detrimental effects of the liquid metal occurring before the maximum creep allowed in a reactor design is achieved is small [15]. Mechanical property assessments of the candidate materials are important for the design of ADS. No investigation on LME has shown that O in LBE can prevent LME. Most studies were performed at low oxygen potential or it was not measured at all. Yurechko et al. found that creep and stress rupture properties may not degrade in the presence of solved oxygen, but this is for Pb [16, 17]. The mechanism of LME is not clear at present, though there are approaches to mechanisms [18]. There is some correspondence to other liquid metals [19, 20]. LME is dependent on many parameters, including strain rate, temperature, stress concentration and surface state. In some conditions, no LME phenomenon was found [21]. Experiments have been carried out to assess the tensile properties of candidate cladding materials in LBE under different strain rates and

temperatures, 150-450 °C in [8], 250-425 °C in [22], 160 °C in [23], 350 °C in [24], and 200-550 °C in [25]. It was found that the tensile properties of T91 deteriorate in liquid metal environment [26]. However, data on the mechanical properties after exposure to LBE for different durations are scarce. It was reported that, whatever the surface state was, with oxide formed during exposure at 923 K, with Pb-Bi locally adhering to the steel surface (at higher than 873 K) or not (at lower than 573 K), the room temperature ductility of T91 steel was unaffected [27].

Beside LME, the steels will suffer from corrosion and oxidation from LBE when serving under high temperature. It was reported in a study in the temperature range of 420-540 °C that the protection means against the dissolution of the steels is the in situ protection by the formation of an oxide layer on the surface of the steel [28]. In this way, an oxide layer is formed when the steel becomes in contact with the LBE, akin to the self-repair mechanism of stainless steel in atmospheric conditions.

It was reported that the Russian martensitic steel with 1.8 % Si exhibited good corrosion resistance in flowing LBE [29-32]. It is known that the Si addition to steels increases oxidation resistance in gas environment [29]. Investigations by Van den Bosch et al., however, indicate that Si is detrimental in respect of LME [25]. The effects and role of Si are not confirmed or understood sufficiently in liquid Pb-Bi environment.

Aging degraded the ductility of T91 [33]. $M_{23}C_6$ carbide coarsening and lath microstructure degradation to equiaxed sub-grain structure before the formation of Z-phase lead to the significant breakdown of stress rupture limit and low hardness, which is the main cause for the T91 tube bursting [34].

Examining the temperatures or temperature range covered by previous studies, information is missing for higher temperatures, for example 600 °C. This is a uniqueness of the present investigation. The aim of the work is to contribute to the development of critical materials, especially in relation to those requiring satisfactory mechanical properties, for the next generation nuclear power plants. The objective of the research is to find out the influence of exposure to LBE and the LBE oxidation on the tensile behavior of F/M steels. For comparison purposes, tensile tests were conducted after aging and contacting LBE for same lengths of time. The aim of the experiments was to tell effects of thermal ageing from effects of LBE.

2. Experimental

2.1. Material characteristics

Two F/M steels were employed in this research. One was T91 steel, and the other was the newly developed SIMP steel. The SIMP steel was melted in a 500 kg vacuum induction melting furnace. The T91 steel was commercially produced by Sumitomo Metal Industries,

Japan, and so not melted locally. The chemical compositions of the experimental steels, measured using inductively coupled plasma (ICP) optical spectrometer (TCH 600), are shown in Table 1. The average grain size of T91 steel is about 9 μm and that of SIMP steel is about 20 μm. In SIMP, the activating element Ni is removed. In order to improve the creep behavior, the Cr and Ni equivalent is controlled to obtain a martensitic single-phase microstructure. The particular elements acting equivalently in respect of martensite formation can be considered using a chrome equivalent (Cr + Mo + 1.5Si + 0.5Nb, the coefficient giving weightings according to the effectiveness of the elements). The nickel and manganese, on the other hand, form austenite. It is preferable to balance, e.g., removing Ni but adding Mn, which may be seen from comparing the compositions of T91 and SIMP steels. The higher Cr content provides SIMP with good oxidation resistance. Two recently published papers describe in more detail the SIMP steel with its composition modifications from T91 [35, 36]. Experiments were carried out to optimize the normalization and tempering heat treatment of SIMP, based on best mechanical properties viz. strength and toughness. However, these were not published, and are outside the scope of the present paper.

Table 1. Chemical compositions of the experimental steels (wt%)

Steel	C	Cr	Ni	Ta	Mo	W	Mn	Si	V	Nb	N
T91	0.1	8.4	0.1	-	0.9	-	0.4	0.2	0.2	0.04	0.05
SIMP	0.2	10.7	-	0.1	-	1.2	0.5	1.4	0.2	0.01	0.013

2.2. Heat treatment

The T91 specimens were cut from tubes produced by Sumitomo Metal Industries Ltd. The outer diameter of the T91 tubes was 64 mm and inner diameter was 46 mm. The T91 steel was normalized at 1323 K for 20 min, and then tempered at 1053 K for 60 min. After being rolled into plates of 14 mm thickness, the SIMP steel was normalized at 1323 K for 30 min, and then tempered at 1033 K for 90 min. Air cooling was used. No steps were taken to control the cooling rate. The martensite microstructure will form through air cooling, so water quenching was not applied. The cooling rate after each stage of the heat treatment, was estimated at about 300 K/min. The microstructure of both steels consists only of tempered martensite, plus the inevitable carbides. The latter play also a role on mechanical performance. Micrographs were taken. A quantitative analysis of grain size was carried out.

2.3. Tensile testing

The specimens after heat treatment were divided into two groups. After aging in furnace for different durations, the specimens of the aging group were machined for tensile test. The other group of specimens were machined as tensile specimens and exposed to LBE for the same duration with aging groups, as shown in Fig. 1. The tensile tests were carried out after extracting tensile specimens from LBE. The tensile curves after aging and after exposure to LBE are presented in one graph for comparison.

Cylindrical tensile specimens with gauge length of 25 mm and diameter of 4 mm were machined. The overall length of the tensile specimens was 60 mm. The tensile specimens were not ground before test. The surface was in as machined state. The cylindrical tensile specimens were tested using a Shimadzu AGX-250kN machine. The constant displacement rate tensile tests were performed at room temperature and 873 K under displacement-control condition with a constant cross-head displacement rate corresponding to a target strain rate of 3.3×10^{-4} s^{-1}. Two specimens were used per test condition. The extensometer could not be used well after reaching yield point during the high temperature tensile testing, so the tensile results are shown using stress-displacement curves, as exact strain data are not available. The displacement is from the tensile machine reading instead of from extensometer measurements, for high temperature testing. The traverse displacement was recorded and considered as characteristic for the elongation of the specimen, for the comparison of specimens tested in the identical machine, with identical geometry. For room temperature tensile testing using extensometer, the elongation was measured from stress-strain curves. For high temperature testing without using extensometer, the elongation was measured manually off the broken tensile specimens.

In order to compare with the effect of thermal aging on the mechanical properties, both steels were aged in a furnace at 873 K for 500 h, 1000 h and 2000 h. The thermally aged samples were machined into tensile specimens and tensile tests were performed.

Extensive tensile testing was also carried out after exposing the steel tensile specimens to LBE. The exposure process is described in the next section. The tensile testing process for the LBE exposed specimens is as described above in this section.

2.4. Exposure to LBE

The fresh tensile specimens were exposed to the LBE. In addition, small square corrosion specimens with dimension of 10×10×5 mm^3 were ground up to 2000# abrasive paper and polished using a polishing solution containing 2.5 μm particles for 15 min, and then immersed in the LBE at 873 K together with those tensile specimens, for the purpose of observing the oxidation layer on the surface. The corrosion specimens were machined using the same material as tensile specimens. Both the corrosion specimens and tensile specimens were in contact with LBE under the same condition for the same duration.

The liquid lead–bismuth alloy used in the test was at the eutectic composition, 55.5 wt% Bi and 44.5 wt% Pb. The liquid LBE is greatly purified. The trace contents of impurities are Mg, Al, Cr, Ni, Cu, Zn, As, Sb, Cd each < 1 ppm, Sn < 3 ppm, Fe, Ag each < 5 ppm, Si < 10 ppm. There are no C or N contents in the LBE. LBE of high purity was purchased. No purification was performed in the laboratory. The molten eutectic was saturated with oxygen at 873 K before the exposure of the specimens. The oxygen saturation process, at 873 K, was explained in a previous paper [35]. In that paper, it is stated that air covers the surface of the liquid and oxygen saturation was deduced from the presence of PbO floating on the surface.

This is qualitatively different from measurements with an oxygen sensor. It can be clearly stated that the liquid was saturated with oxygen close to the surface. In the bulk of the LBE, oxygen concentration may have been different, especially lower than saturation. The number of specimens, their surface area, possibly also the surface of the containment if made of steel may have an effect. After exposure to LBE, the oxygen distribution is homogenous along the gauge of specimens. A previous paper [35] shows pictures to demonstrate that the oxidation scale along gauge is homogenous in SIMP and T91 formed in static LBE. The oxygen distribution is not homogenous across the gauge of specimens. There are many sub-layers and different oxygen contents are observed. The oxygen content is calculated as 3.7×10^{-3} wt% according to the equation $\lg c_{O[Pb\text{-}Bi]sat.} = 2.62 - 4416/T$ (600 K < T < 1073 K), where T is the temperature [37]. A schematic diagram is shown in Fig. 1. In this experiment, the vessel, which contains the liquid metal, the force bar and specimen holder are made of a 9-12 Cr steel, as reported in [35]. Different components were machined by electrical discharge machining and welded to form the specimen holder. The surface finishing state of container of LBE has no effect on the corrosion/oxidation behavior of steel in LBE, as proved in [38]. More details of test set-up can be found in [35]. The tensile specimens were fixed in a holder and forced into the LBE melt. The square corrosion specimens and the gauge of tensile specimens were in direct contact with the LBE. The exposure times are 500 h, 1000 h and 2000 h. There was no means to control the atmosphere during the exposure and tensile test. There are no oxygen concentration sensors in this experimental set-up. In the actual ADS, there are many means to maintain the oxygen concentration at a constant. The oxygen concentration is monitored on line. The actual condition in ADS is different from the nominal

condition here. In this investigation, the LBE melt was exposed to air. The oxygen had enough time to dissolve and diffuse in LBE until a saturated state was reached. The duration of samples contacting with LBE was very long. The LBE was oxygen-saturated as in previous tests performed using the same equipment and under the same atmosphere. More details can be found in [35]. Oxygen is also considered to be saturated in [39]. The LBE is saturated with oxygen if there are no steps to control the surrounding atmosphere.

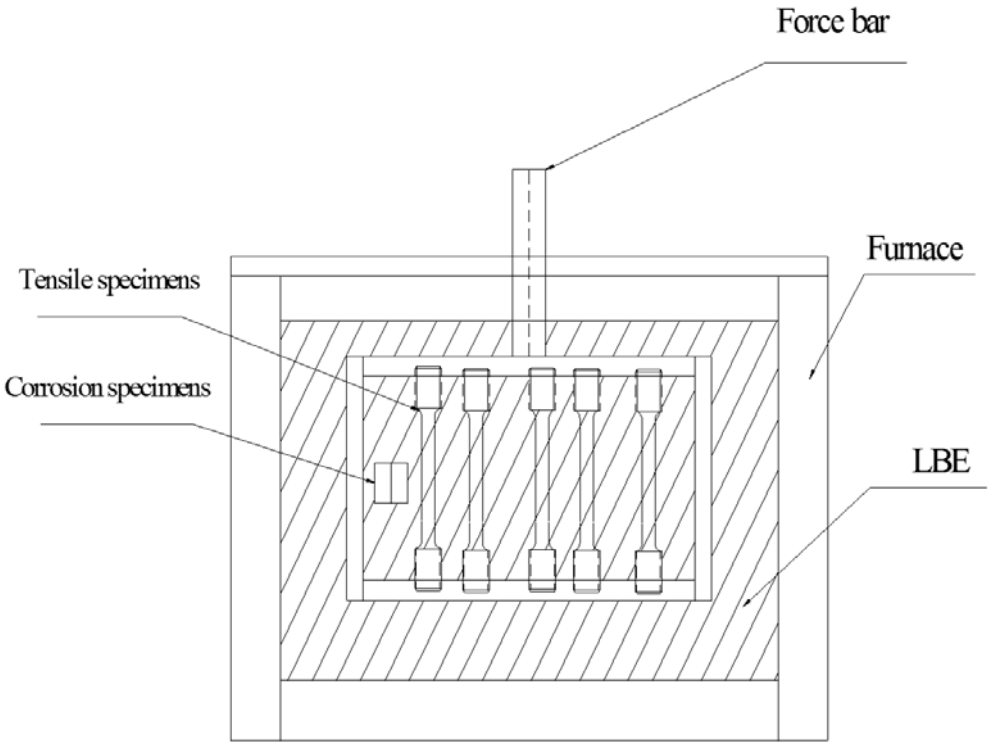

Fig. 1. Schematic diagram of test set-up.

After being taken out from the melt alloy, the tensile specimens were put in hot edible tea oil at about 473 K to remove the residual LBE. This tea oil has a high boiling point.

2.5. Metallography and fractography

After extraction from the melt, the corrosion coupons were cleaned in hot edible oil at about 473 K to remove adherent LBE. The corrosion specimens were then cut, mounted, ground, polished, and etched using Vilella's reagent (1 g of picric acid, 5 ml 37.5% hydrochloric acid in 100 ml ethyl alcohol) for microstructural analysis on the cross-section using optical microscopy (OM) and scanning electron microscopy (SEM). The above procedures were also carried out for cross-section study of tensile specimens, but not on the fracture surface. The fracture surface was examined. Both the surface and cross section of the small square corrosion specimens were investigated.

3. Results and discussion

3.1. Microstructure

The original and the aged microstructures of T91 and SIMP steels are shown in Fig. 2. The influence of aging treatment on microstructures of the two steels is minimal. The martensitic laths show no change, at least at the magnification in Fig. 2. The etching process by Vilella's reagent is not very effective on T91 and the microstructure is not very clear. The original microstructure of T91 was thus observed under SEM at higher magnification (Fig. 3). The elements in precipitates were also analyzed. Some large carbides, such as the one indicated in Fig. 3c are $Cr_{23}C_6$. Many carbides precipitate along grain boundaries. Cui et al. investigated

mechanical properties of T91 after aging for 3000 h, 5000 h and 8000 h at 600 °C [40]. There is no mechanical strength degradation. After long-term aging, the Laves phase precipitates.

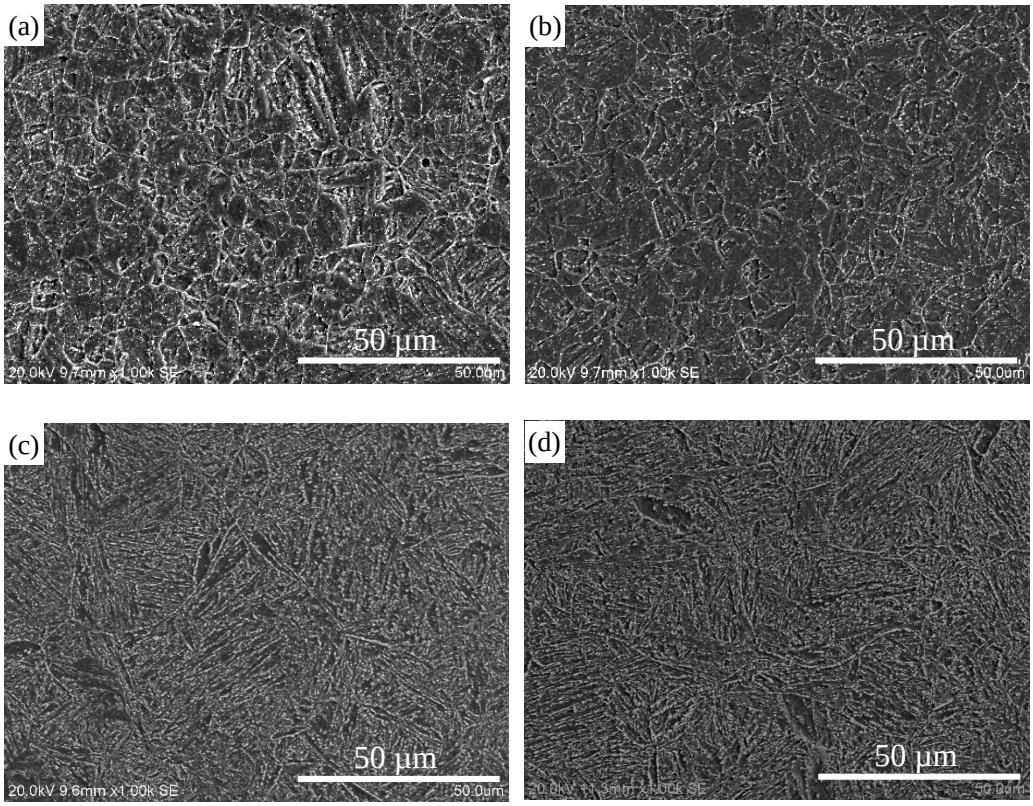

Fig. 2. Original and aged microstructures of the experimental steels. (a) Original T91; (b) T91 aged at 873 K for 2000 h; (c) original SIMP; (d) SIMP aged at 873 K for 2000 h.

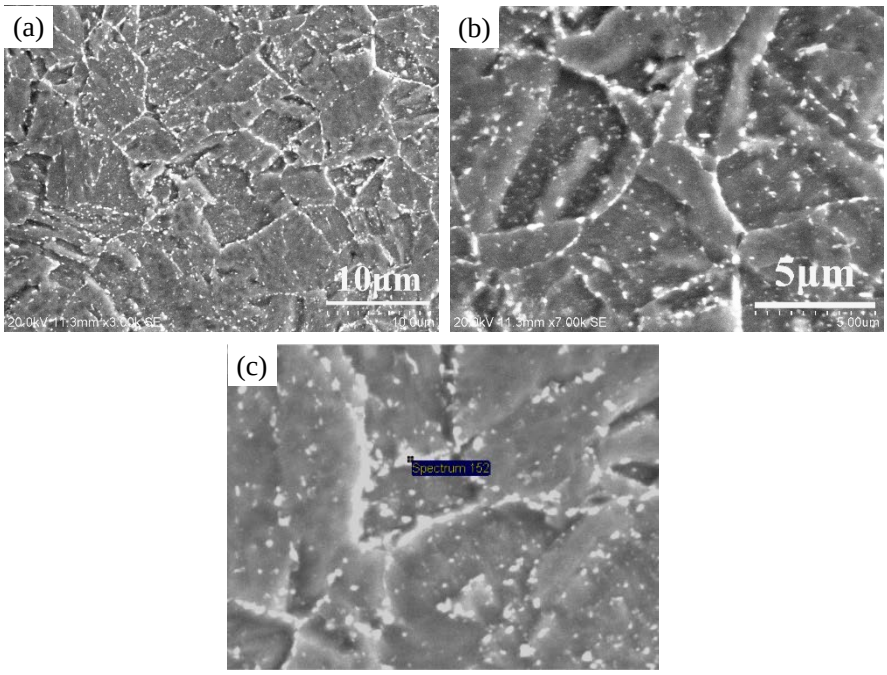

Fig. 3. Original microstructure of T91 without aging.

3.2. Tensile properties

The tensile strength of the T91 steel at 873 K is 343 MPa, with elongation 39%, in tempered state (Fig. 4a). Under this condition, the tensile strength of the SIMP steel at 873 K is 358 MPa, with elongation 44% (Fig. 4b). There are no significant changes in the tensile properties of the two steels after aging for different times. The strength and elongation (Table 2) of the two steels remain nearly the same after aging, compared to before aging. Therefore, the thermal stability of the two steels is good during short-term aging. The results from the tensile tests are linked to the microstructure after aging. In fact, this corroborates the notion that changes in microstructure after aging are minor.

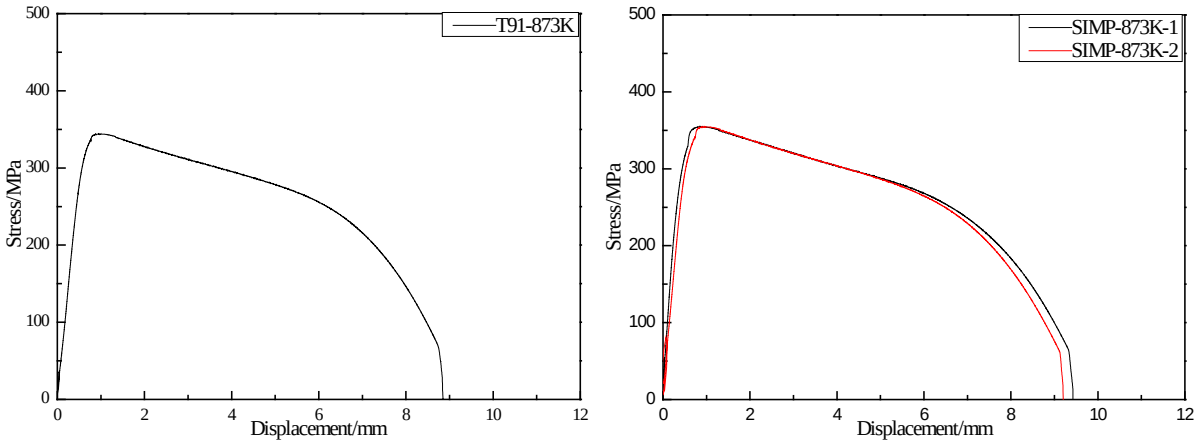

(a) (b)

Fig. 4. Tensile curves of the experimental steels at 873 K, before aging or exposure to LBE. (a) T91, (b) SIMP, showing results from two specimens. Extensometers were not used in tensile tests at 873 K.

Comparison of the tensile curves between the specimens exposed to LBE and after aging shows that the elongation of the steels is reduced after immersion in the liquid metal (Fig. 5). Fig. 5 exemplifies the tensile curves using exposure for 500 and 1000 h as examples. The tensile curves after aging or exposure to LBE for other times have similar shapes, for the respective steels. When tensile tested at room temperature, for both steels, the degradation in strength after exposure LBE is observed compared to after aging in argon. The total elongation remains unchanged. When tensile tested at 873 K, the reduction in elongation after exposure to LBE for different lengths of time is similar. The strength of the steels degraded slightly after exposure to LBE (Table 2). There is a trend that degradation of strength increases with increasing exposure time to LBE (Fig. 6).

Table 2. Yield strength (YS), ultimate tensile strength (UTS) and total elongation before and after aging or exposure to LBE at 873 K

Steel	Test temperature	Aging or LBE at 873 K (h)	YS after aging (MPa)	YS after LBE (MPa)*	UTS after aging (MPa)	UTS after LBE (MPa)	Elongation after aging (%)	Elongation after LBE (%)
T91	RT	0**	514±2	514±2	687±1	687±1	27.4±0.1	27.4±0.1
		500	509±6	477±2 (515)	679±3	628±2	27.3±0.4	26.5±0.6
		1000	515±8	460±1 (509)	687±8	598±2	27.0±0.0	27.3±0.1
		2000	515±3	461±3	684±3	607±1	25.0±0.7	24.8±0.2
	873 K	0**	309±13	309±13	343±2	343±2	39.3±0.4	39.3±0.4
		500	312±1	309±7	351±5	341±12	38.5±1.4	35.2±0.4
		1000	317±2	283±1	347±2	325±3	38.8±1.8	18.8±0.6
		2000	305±1	285±7	344±3	332±9	39.8±6.7	21.0±0.7
SIMP	RT	0**	609±1	609±1	835±1	835±1	23.5±0.7	23.5±0.7
		500	589±20	556±6 (585)	831±13	775±8	23.9±1.5	23.4±0.1
		1000	609±9	550±1 (594)	836±6	757±5	24.0±0.0	23.5±0.2
		2000	603±2	559±6	835±4	766±6	23.0±0.0	23.5±0.3
	873 K	0**	293±4	293±4	358±4	358±4	44.0±1.4	44.0±1.4
		500	303±9	285±3	356±2	347±3	46.5±2.1	37.5±0.7
		1000	309±7	281±8	361±7	340±5	48.0±2.8	36.5±4.4
		2000	296±2	286±3	353±2	346±11	47.5±3.5	28.1±0.0

*Recalculated values using the reduced cross section area, taking into account the material loss due to oxide scale formation, are shown in brackets. Only a few cases were recalculated, as this is for illustration purposes.

**Results under “after aging” and under “after LBE” are from identical tests, as the aging or the exposure time is 0.

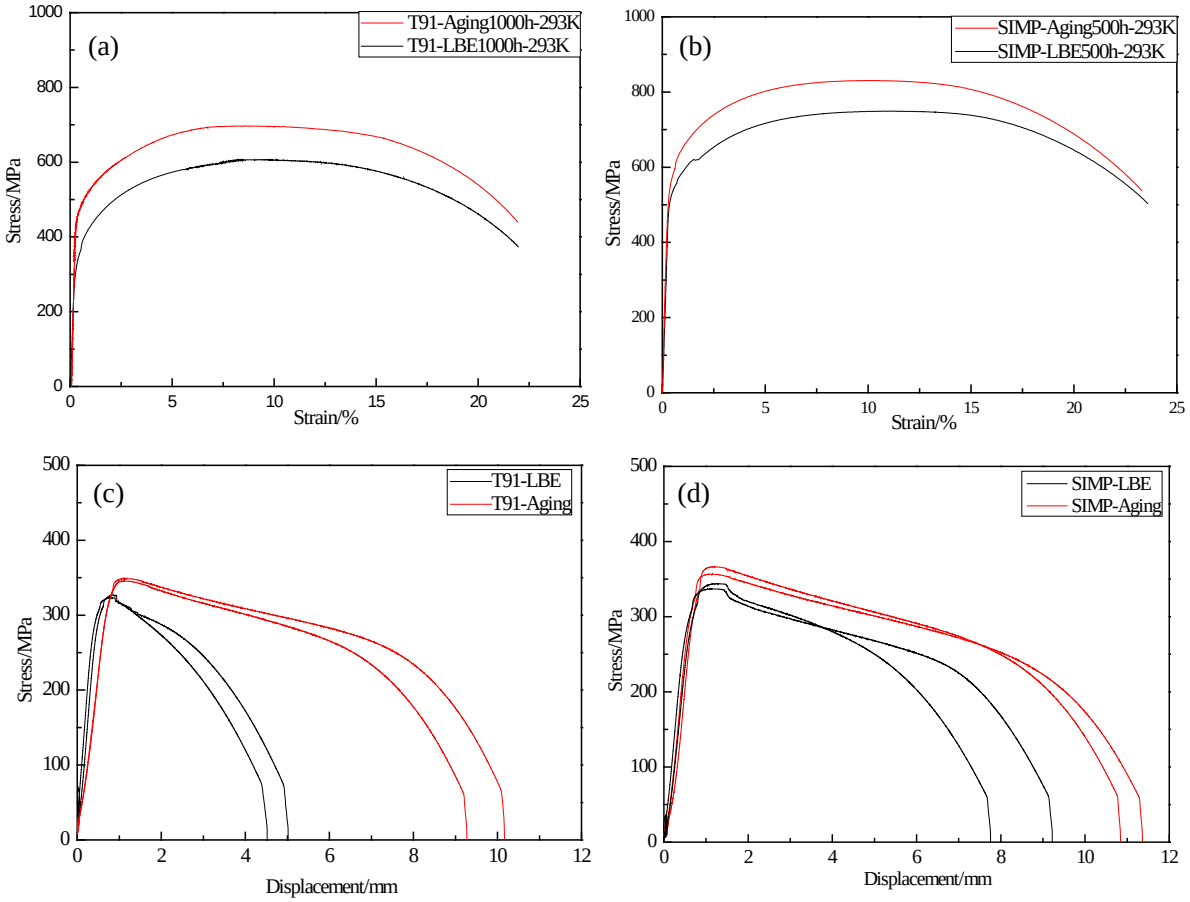

Fig. 5. Tensile curves of the experimental steels at (a,b) room temperature and (c,d) 873 K (two test curves shown per condition, after aging and exposure to LBE for 1000 h). (a,c) T91, (b,d) SIMP.

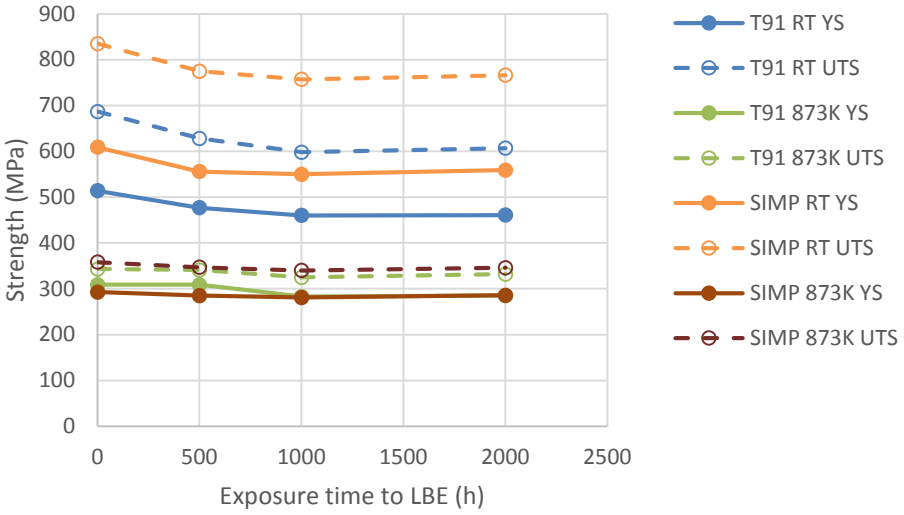

Fig. 6. Strength (at room temperature and 873 K) as a function of exposure time to LBE (at 873 K).

Hojná et al. reported that LME was not found on any of the smooth specimen tested in liquid Pb [41]. A thin oxide layer appeared on the specimen surface after the tensile tests which would have to be broken in order to ignite the LME crack initiation. With respect to that, the uniaxial test condition, i.e. slow loading up to tensile strength followed by necking, is not sufficient to stimulate LME of the T91 in the liquid Pb.

3.3. Oxide layers

The cross-sections of oxidation layer are shown in Fig. 7. The oxidation layer consists of outer (labeled O in Fig. 7) and inner (labeled I in Fig. 7) layers. The outer oxidation is porous and inner oxidation layer is dense. The morphology of the oxide layer after 2000 h is similar to that after 1000 h. The morphology after 500 h exposure also has similar patterns, but the oxidized layers are thinner. Si addition has resulted in better oxidation resistance [29-32]. Oxide layer of SIMP is thinner than T91 [35], but the effects of Si are not confirmed and understood sufficiently in liquid Pb-Bi environment. The effects of Cr on oxidation layer of SIMP are presented in [35].

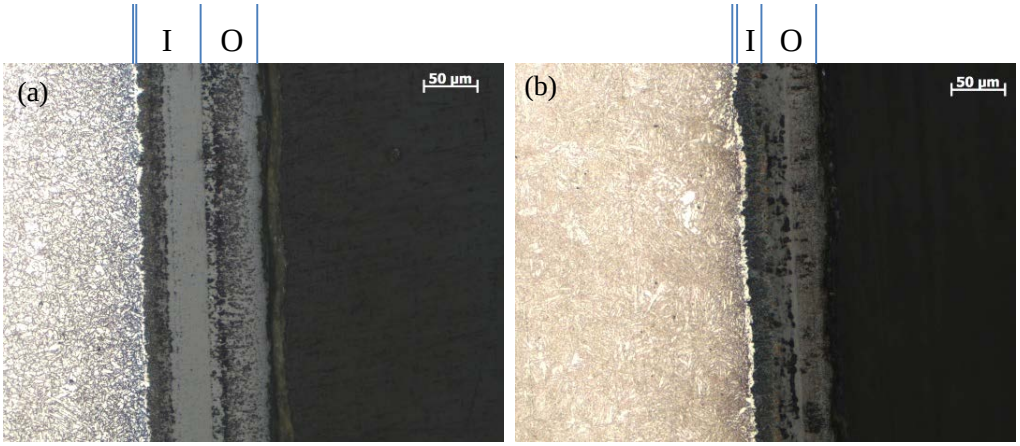

Fig. 7. Oxidation layers after 1000 h pre-exposure, etched by Vilella's reagent. (a) T91, (b) SIMP.

In Fig. 7, it can be found that there is a white layer (the thin, unlabeled layer immediately to the left of the inner layer in Fig. 7) between the oxidation layer and the steel. Generally, the white layer is more pronounced for the SIMP steel. It is about 3 µm thick and not visible before etching by Vilella's reagent. The concentrations of Cr and Si are low in this layer measured by EDS and EMPA, as shown in [35]. The lower Cr and Si content indicates a depletion zone that is etched differently from the bulk of the steel – possibly due to a transformation of the martensite into ferrite though there is no firm evidence at present. The SEM shows the ferrite like morphology. The Cr and Si contents are lower than in the steel and oxidation layer. We have no facility to accurately detect C depletion as well. It is possible that Cr and Si in this layer diffused outward from steel during the oxidation layer formation, and carbon reacted with oxygen and left the steel, but there is no confirmation of these at present. More detailed information and description of the layers can be found in [35].

The scale thickness was measured from cross sectional micrographs, from which the reduction in cross section was estimated. The reduction of cross section was determined equal to the cross section area of the scales.

Ref. [35] presents the elemental analysis of cross-section of the oxidation layer, showing that the oxygen diffused into the steel, resulting in internal oxidation. The oxygen atoms reacted with Cr and Si to produce spinel in the inner oxidation layer. The elemental analysis, having already been published in [35] for the research shown in that paper, is not repeated here, but is used here to enable discussion. No property measurement data was available previously, however.

As presented in Fig. 8, the oxidation layer formed on the surface is brittle and may flake off and spall off from the steel under stress. The pre-formed oxide scale cracks and locally detaches during the tensile test. This is as expected in view of typically lower ductility of oxides in comparison to steels. The residual LBE will then be in contact with steel.

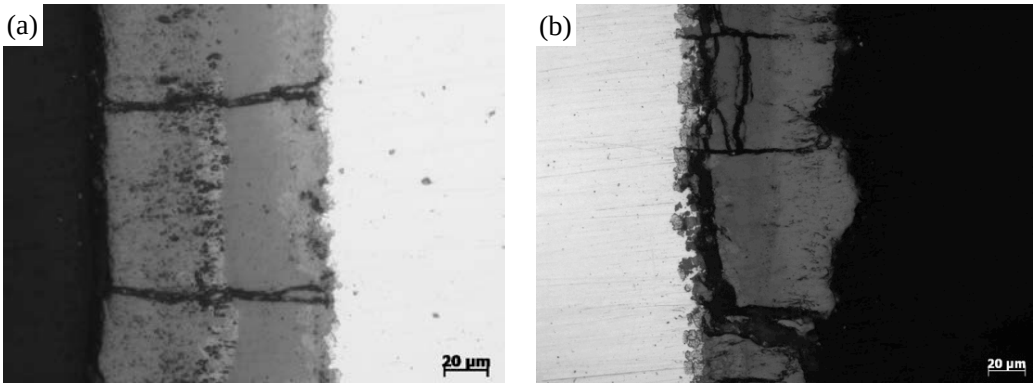

Fig. 8. Cross-section of tensile specimens after pre-exposure to LBE for 2000 h. (a) T91; (b) SIMP. The areas examined here are far away from the tensile fracture locations. The oxide layer near the fracture all spalled off.

The surface morphologies of outer oxidation layer on the experimental steels are shown in Fig. 9. It can be seen that the outer oxidation layer is porous. So, it should be easy for the liquid metal LBE to attach and permeate, at high temperature, into the outer oxidation layer. Some LBE solidified on outer oxidation layer and re-melted during tensile testing at 873 K and permeated to contact steel.

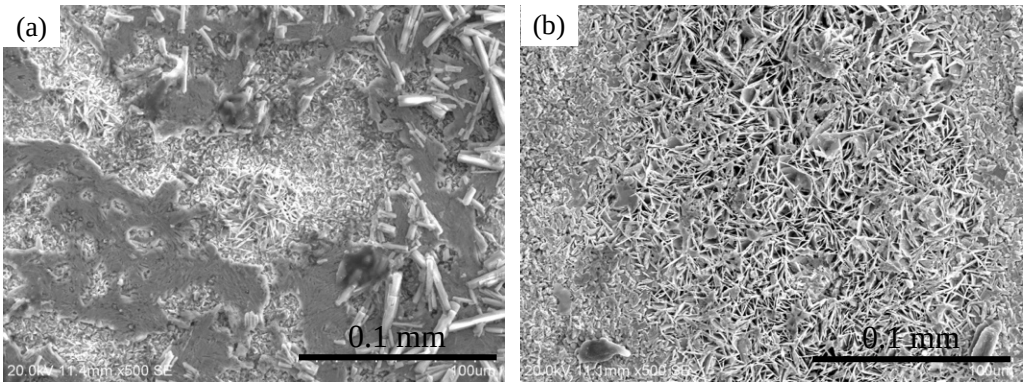

Fig. 9. Surface morphology of outer oxidation layer on corrosion coupons of the experimental steels after pre-exposure to LBE for 1000 h. (a) T91; (b) SIMP.

Backscattered electron micrographs show the permeation of heavy metal locally at the peripheral part of fracture surfaces (near the surface of the tensile specimens, i.e., the edges of the cone-shaped fracture surface). The location of LBE permeation shows brittle fracture character, as seen in Fig. 10. The center of the fracture surface reveals dimples. In contrast, the zones of LBE penetration show no dimples at the peripheral of fracture surfaces. Schmidt et al. found the ductility loss at the periphery and ductile fracture at the center of their tensile test specimens [42]. Glasbrenner and Viol found the penetration of LBE into MANET II steel [43]. Aiello et al. found that the fracture surface exhibited a mixed ductile and brittle morphology after T91 specimens were exposed to LBE for 4500 h at 450 °C. The penetration of the liquid metal element may be one of the reasons of the degradation of the mechanical properties [44]. The BSE images in Figs. 10c and f show the location of heavy metal LBE clearly. The BSE micrographs show the permeation of heavy metal locally at the peripheral part of fracture surfaces. The locations of LBE permeation show brittle fracture character (Figs. 10b and e). This is the possible reason for the elongation reduction. The internal oxidation reduces the load-bearing cross section, leading to degradation in strength. The elongation decreases at 873 K but does not deteriorate at room temperature. So, the embrittlement is not caused by internal oxidation. The oxide cracks, but cracking is not into the steel.

3.4. Oxide scale and tensile load

The reduction in cross-section is deduced from the oxide thickness measurement, same in the coupon tests and on the tensile specimens, naturally performed after the tensile test. In the latter, the examination shows that the oxide layer cracked (Fig. 8).

The oxide scale did not bear tensile load for the following reasons. Firstly, according to a previous investigation [39] and hardness measurement results (Fig. 11), the oxide scale is much harder than the steel matrix. It indicates that the elongation of oxide scale is much smaller than steel.

Secondly, the observation on the surface and cross section of specimens reveals porous feature in external oxidation layer (Fig. 9). It is impossible for such oxide scales to bear the tensile load.

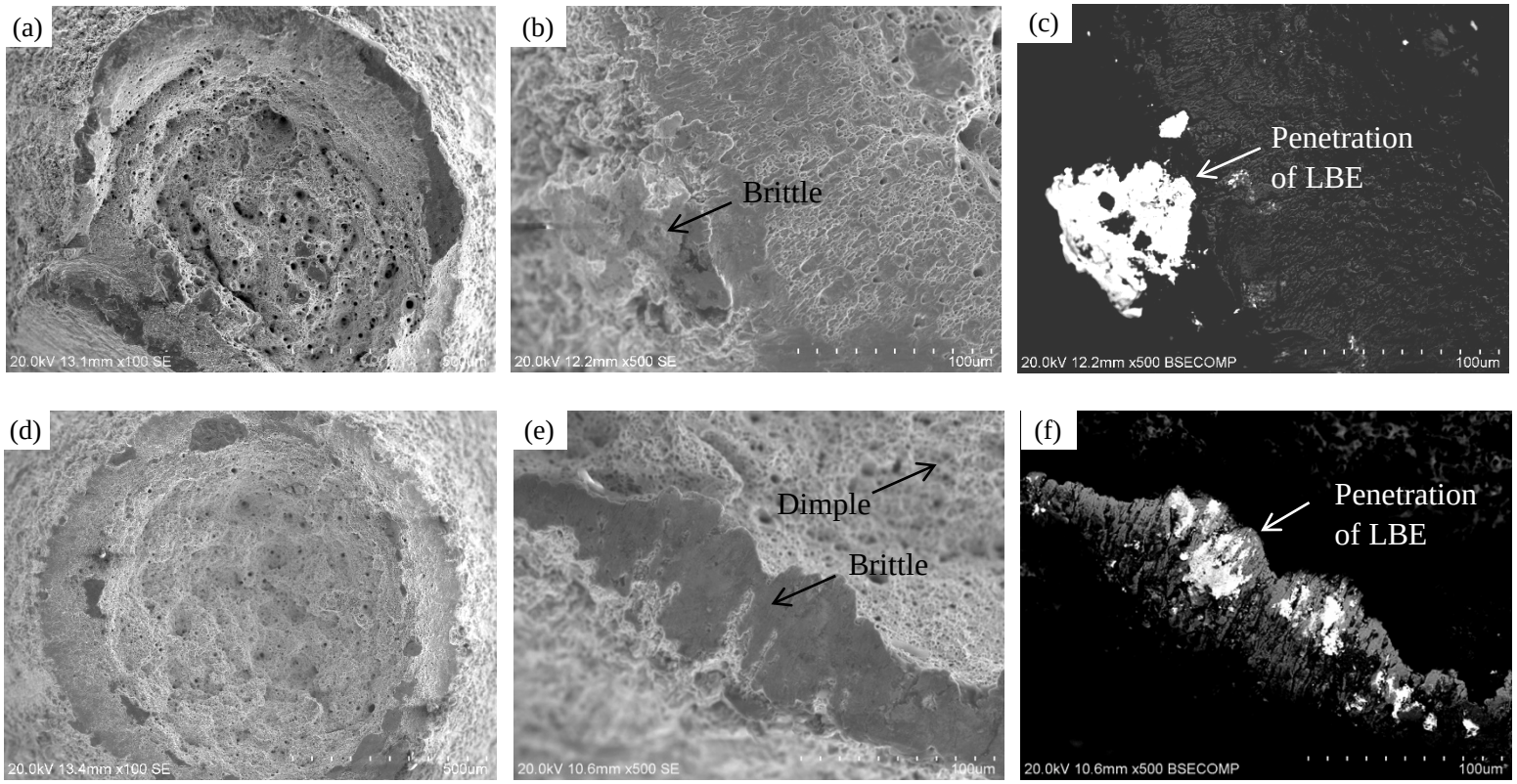

Fig. 10. Morphologies of (a,d) the whole tensile fracture surfaces and (b,c,e,f) fracture surfaces at the peripheral part of tensile specimens. (a,b) T91 secondary electron image; (c) T91 BSE; (d,e) SIMP secondary electron image; (f) SIMP BSE.

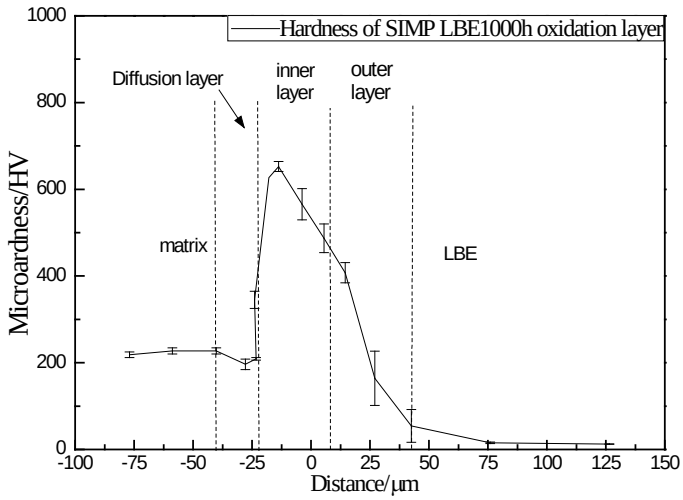

Fig. 11. Vickers hardness depth profile of SIMP.

Thirdly, the oxide scales were ruptured and peeled off under tensile loading, on ruptured tensile specimens. The internal oxidization reduces the cross section, i.e., the solution of elements contributes to the loss of cross section, but external oxidization increases the cross section area.

There is no degradation in tensile properties of the two ferritic/martensitic steels after aging for 500 h, 1000 h and 2000 h. The aging for short times causes no significant deterioration on mechanical properties of both steels. So, the degradation of mechanical properties is attributed to the oxide scale.

The engineering stress is calculated by dividing the load by cross section area of tensile specimen’s gauge. The cross section consists of steel and oxide scale. The oxide scale is ruptured under tensile load, before the rupture of steel. So, the strength of both steels decreases.

4. Conclusion

Aging at 873 K for up to 2000 h has no great influence on the mechanical properties of two F/M steels, T91 and SIMP. After pre-exposure to LBE, the oxidation layer reduces the steel cross-sectional area of the tensile specimens, and so the tensile strength of specimens decreases. On 4 mm diameter specimens, when tested at 873 K after 2000 h exposure, the tensile strength of T91 decreases from 343 MPa to 332 MPa, and elongation from 39% to 21%. For SIMP, the decreases are from 358 MPa to 346 MPa and from 44% to 28%, for tensile strength and elongation, respectively. The room temperature strength has slightly larger percentage reductions after the LBE exposure, but the elongation changes little.

Acknowledgments

This work was financially supported by a sub topic (XDA03010301, XDA03010302) of the Advanced Fission Energy Program-ADS Transmutation System, Chinese Academy of Sciences Strategic Priority Research Program (XDA03010000).

References

[1] H. Oigawa, K. Tsujimoto, K. Nishihara, T. Sugawara, Y. Kurata, H. Takei, S. Saito, T. Sasa, H. Obayashi, J. Nucl. Mater., 415 (2011) 229-236.

[2] A. Ahmad, S.J. Steer, G.T. Parks, Energy Convers. Manage., 69 (2013) 181-190.

[3] C. Fazio, I. Ricapito, G. Scaddozzo, G. Benamati, J. Nucl. Mater., 318 (2003) 325-332.

[4] J. Van den Bosch, A. Almazouzi, G. Mueller, A. Rusanov, J. Nucl. Mater., 415 (2011) 276-283.

[5] M.B. Toloczko, F.A. Garner, C.R. Eiholzer, J. Nucl. Mater., 212 (1994) 604-607.

[6] J. Zhang, N. Li, J. Nucl. Mater., 373 (2008) 351-377.

[7] P. Hosemann, R. Dickerson, P. Dickerson, N. Li, S.A. Maloy, Corros. Sci., 66 (2013) 196-202.

[8] J. Van den Bosch, D. Sapundjiev, A. Almazouzi, J. Nucl. Mater., 356 (2006) 237-246.

[9] S. Hemery, T. Auger, J.L. Courouau, F. Balbaud-Celerier, Corros. Sci., 76 (2013) 441-452.

[10] G. Nicaise, A. Legris, J.B. Vogt, J. Foct, J. Nucl. Mater., 296 (2001) 256-264.

[11] J. Liu, Q. Huang, Z. Jiang, Z. Zhu, M. Li, Fus. Eng. Des., 88 (2013) 2603-2606.

[12] D. Gorse, T. Auger, J.B. Vogt, I. Serre, A. Weisenburger, A. Gessi, P. Agostini, C. Fazio, A. Hojna, F. Di Gabriele, J. Van den Bosch, G. Coen, A. Almazouzi, M. Serrano, J. Nucl. Mater., 415 (2011) 284-292.

[13] Yongwei Sun, Jizhi Chen, Jun Liu, Mater. Sci. Eng. A, 625 (2015) 89-97.

[14] Mala M. Sharma, Josh D. Tomedi, Timothy J. Weigley, Mater. Sci. Eng. A, 619 (2014) 35-46.

[15] Robert Petroski, Benoit Forget, Charles Forsberg, Ann. Nucl. Energy, 55 (2013) 151-168.

[16] M. Yurechko, C. Schroer, A. Skrypnik, O. Wedemeyer, J. Konys, J. Nucl. Mater., 450, (2014) 88-98.

[17] M. Yurechko, C. Schroer, O. Wedemeyer, A. Skrypnik, J. Konys, Nucl. Eng. Des., 280 (2014) 686-696.

[18] May Martin, A new approach to discovering the fundamental mechanisms of hydrogen failure, PhD thesis, University of Illinois at Urbana-Champaign, 2013.

[19] M.L. Martin, T. Auger, D.D. Johnson, I.M. Robertson, J. Nucl. Mater., 426 (2012) 71-77.

[20] J. Luo, H. Cheng, K.M. Asl, C.J. Kiely, M.P. Harmer, Science, 333 (2011) 1730-1733.

[21] C. Beal, X. Kleber, D. Fabregue, M. Bouzekri, Scripta Mater., 66 (2012) 1030-1033.

[22] Y. Dai, B. Long, F. Groeschel, J. Nucl. Mater., 356 (2006) 222-228.

[23] Z. Hamouche-Hadjem, T. Auger, I. Guillot, D. Gorse, J. Nucl. Mater., 376 (2008) 317-321.

[24] T. Auger, G. Lorang, S. Guérin, J.-L. Pastol, D. Gorse, J. Nucl. Mater., 335 (2004) 227-231.

[25] J. Van den Bosch, G. Coen, P. Hosemann, S. Maloy, J. Nucl. Mater., 429 (2012) 105-112.

[26] Jian Liu, Wei Yan, Wei Sha, Wei Wang, Yiyin Shan, Ke Yang, J. Nucl. Mater., 473 (2016) 189-196.

[27] C. Fazio, Handbook on lead-bismuth eutectic alloy and lead properties, materials compatibility, thermal-hydraulics and technologies, OECD/NEA (Organisation for Economic Cooperation and Development/Nuclear Energy Association), 2007.

[28] L. Martinelli, J.-L. Courouau, F. Balbaud-Célérier, Nucl. Eng. Des., 241 (2011) 1288-1294.

[29] Y. Kurata, M. Futakawa, J. Nucl. Mater., 325 (2004) 217-222.

[30] F. Barbier, A. Rusanov, J. Nucl. Mater., 296 (2001) 231-236.

[31] G. Benamati, C. Fazio, H. Piankova, A. Rusanov, J. Nucl. Mater., 301 (2002) 23-27.

[32] G. Muller, G. Schumacher, F. Zimmerman, J. Nucl. Mater., 278 (2000) 85-95.

[33] Y. De Carlan, A. Alamo, M. Mathon, G. Geoffroy, A. Castaing, J. Nucl. Mater., 283 (2000) 672-676.

[34] X. Wang, X. Zhang, L. Zhan, Y. Ren, Proceedings of the Chinese Society of Electrical Engineering, 32(29) (2012) 137-142.

[35] Q. Shi, J. Liu, H. Luan, Z. Yang, W. Wang, W. Yan, Y. Shan, K. Yang, J. Nucl. Mater., 457 (2015) 135-141.

[36] J. Liu, Q. Shi, H. Luan, W. Yan, W. Sha, W. Wang, Y. Shan, K. Yang, Oxid. Met. 84 (2015) 383-395.

[37] C. Schroer, A. Skrypnik, O. Wedemeyer, J. Konys, Corros. Sci., 61 (2012) 63-71.

[38] F.J. Martín-Muñoz, L. Soler-Crespo, D. Gómez-Briceño, J. Nucl. Mater., 416 (2011) 80-86.

[39] O. Yeliseyeva, V. Tsisar, G. Benamati, Corros. Sci., 50 (2008) 1672-1683.

[40] Z. Cui, Y. Wang, S. Zhao, Q. Li, Mater. Mech. Eng., 38(12) (2014) 78-81.

[41] A. Hojná, F. Di Gabriele, J. Klecka, J. Burda, J. Nucl. Mater., 466 (2015) 292-301.

[42] B. Schmidt, S. Guerin, J-L. Pastol, P. Plaindoux, J-P. Dallas, C. Leroux, D. Gorse, J. Nucl. Mater., 296 (2001) 249-255.

[43] H. Glasbrenner, D. Viol, Fus. Eng. Des., 61 (2002) 691-697.

[44] A. Aiello, M. Agostini, G. Benamati, B. Long, G. Scaddozzo, J. Nucl. Mater., 335 (2004) 217-221.